

Electrocatalytic water oxidation by copper(II) complexes with pentadentate amine-pyridine ligand

Junqi Lin^{a*}, Nini Wang^a, Xin Chen^a, Xueli Yang^a, Li Hong^a, Zhijun Ruan^a, Hui Ye^a, Yanmei Chen^{a*} and Xiangming Liang^{b*}

^a Hubei Key Laboratory of Processing and Application of Catalytic Materials, College of Chemistry and Chemical Engineering, Huanggang Normal University, Huanggang, 438000 China.

^b Institute for New Energy Materials & Low Carbon Technologies, School of Materials Science and Engineering, Tianjin University of Technology, Tianjin 300384 China.

Email: linjunqi@hgnu.edu.cn, cingym@163.com, liangxm6@163.com

Table S1 Crystallographic data and processing parameters for **1**

Complex parameters	[Cu(MeL)](ClO ₄) ₂ (1)
Empirical formula	C ₁₇ H ₂₅ Cl ₂ CuN ₅ O ₈
Formula weight	561.86
Temperature / K	293(2)
Wavelength / Å	0.71073
Crystal system	Monoclinic
Space group	P2 ₁ /c
<i>a</i> / Å	16.020(8)
<i>b</i> / Å	15.121(8)
<i>c</i> / Å	9.891(5)
<i>α</i> / deg	90
<i>β</i> / deg	102.122
<i>γ</i> / deg	90
Volume / Å ³	2343(2)
<i>Z</i>	4
Calculated density / Mg m ³	1.593
Absorption coefficient	1.213
<i>F</i> (000)	1156
Crystal size / mm	0.22 × 0.20 × 0.18
<i>θ</i> range / deg	2.500 to 21.726
Index ranges	-16 ≤ <i>h</i> ≤ 16 -15 ≤ <i>k</i> ≤ 15 -10 ≤ <i>l</i> ≤ 10
Reflections collected	27747
Independent reflections	2728 [R(int) = 0.1283]
Completeness to <i>θ</i> = 24.792°	98.2 %
Absorption correction	Semi-empirical from equivalents
Max. and min. transmission	0.7446 and 0.4096
Refinement method	Full-matrix least-squares on <i>F</i> ²
Data / restraints / parameters	2728 / 20 / 299
Goodness-of-fit on <i>F</i> ²	1.101
Final R indices [I > 2σ(I)]	<i>R</i> ₁ = 0.0876, <i>wR</i> ₂ = 0.2371
R indices (all data)	<i>R</i> ₁ = 0.1353, <i>wR</i> ₂ = 0.2774
Largest diff. peak and hole	0.715 and -0.416 e.Å ⁻³

$$R_1 = \frac{\sum ||F_o| - |F_c||}{\sum |F_o|}, wR_2 = \left[\frac{\sum (|F_o|^2 - |F_c|^2)^2}{\sum (F_o^2)} \right]^{1/2}$$

Table S2 Crystallographic data and processing parameters for **2**

Complex parameters	[Cu(L)](ClO ₄) ₂ (2)
Empirical formula	C ₁₆ H ₂₃ Cl ₂ CuN ₅ O ₈
Formula weight	547.83
Temperature / K	293(2)
Wavelength / Å	0.71073
Crystal system	Orthorhombic
Space group	Pbca
<i>a</i> / Å	14.9870(3)
<i>b</i> / Å	9.9557(3)
<i>c</i> / Å	29.6358(7)
<i>α</i> / deg	90
<i>β</i> / deg	90
<i>γ</i> / deg	90
Volume / Å ³	4421.84(19)
<i>Z</i>	8
Calculated density / Mg m ³	1.646
Absorption coefficient	1.283
<i>F</i> (000)	2248
Crystal size / mm	0.27 × 0.21 × 0.19
<i>θ</i> range / deg	1.933 to 24.792
Index ranges	-17 ≤ <i>h</i> ≤ 16 -11 ≤ <i>k</i> ≤ 11 -34 ≤ <i>l</i> ≤ 34
Reflections collected	55423
Independent reflections	3797 [R(int) = 0.0710]
Completeness to <i>θ</i> = 24.792°	99.9 %
Absorption correction	Semi-empirical from equivalents
Max. and min. transmission	0.7451 and 0.6188
Refinement method	Full-matrix least-squares on <i>F</i> ²
Data / restraints / parameters	3797 / 20 / 313
Goodness-of-fit on <i>F</i> ²	1.088
Final R indices [I > 2σ(I)]	<i>R</i> ₁ = 0.0830, <i>wR</i> ₂ = 0.2644
R indices (all data)	<i>R</i> ₁ = 0.1044, <i>wR</i> ₂ = 0.2947
Largest diff. peak and hole	1.580 and -0.966 e.Å ⁻³

$$R_1 = \frac{\sum ||F_o| - |F_c||}{\sum |F_o|}, wR_2 = \left[\frac{\sum (|F_o|^2 - |F_c|^2)^2}{\sum (F_o^2)} \right]^{1/2}$$

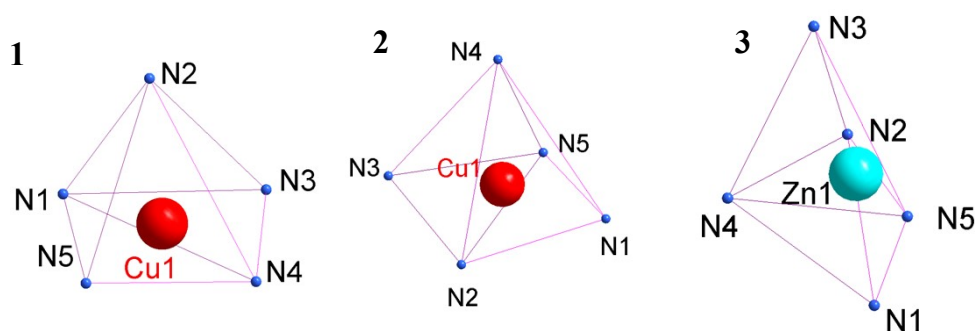
Table S3 Crystallographic data and processing parameters for **3**

Complex parameters	[Zn(L)](ClO ₄) ₂ (3)
Empirical formula	C ₁₆ H ₂₃ Cl ₂ N ₅ O ₈ Zn
Formula weight	549.66
Temperature / K	293(2)
Wavelength / Å	0.71073
Crystal system	Tetragonal
Space group	P4 ₁
<i>a</i> / Å	8.87310(10)
<i>b</i> / Å	8.87310(10)
<i>c</i> / Å	28.4194(6)
<i>α</i> / deg	90
<i>β</i> / deg	90
<i>γ</i> / deg	90
Volume / Å ³	2237.51(7)
<i>Z</i>	4
Calculated density / Mg m ³	1.632
Absorption coefficient	1.389
<i>F</i> (000)	1128
Crystal size / mm	0.22 x 0.20 x 0.17
<i>θ</i> range / deg	2.295 to 27.111
Index ranges	-11 ≤ <i>h</i> ≤ 10 -11 ≤ <i>k</i> ≤ 11 -36 ≤ <i>l</i> ≤ 36
Reflections collected	39361
Independent reflections	4948 [R(int) = 0.0824]
Completeness to <i>θ</i> = 24.792°	100.0 %
Absorption correction	Semi-empirical from equivalents
Max. and min. transmission	0.7455 and 0.6673
Refinement method	Full-matrix least-squares on <i>F</i> ²
Data / restraints / parameters	4948 / 15 / 283
Goodness-of-fit on <i>F</i> ²	1.082
Final R indices [I > 2σ(I)]	<i>R</i> ₁ = 0.1038, <i>wR</i> ₂ = 0.3145
R indices (all data)	<i>R</i> ₁ = 0.1092, <i>wR</i> ₂ = 0.3173
Largest diff. peak and hole	0.893 and -0.917 e.Å ⁻³

$$R_1 = \frac{\sum ||F_o| - |F_c||}{\sum |F_o|}, wR_2 = \left[\frac{\sum (|F_o|^2 - |F_c|^2)^2}{\sum (F_o^2)} \right]^{1/2}$$

Table S4 Selected bond lengths (Å) and angles (deg) for complex **1–3**

Complex	1	2	3	
Bond length (Å)				
Cu–N1	2.051(10)	2.029(6)	Zn–N1	2.115(13)
Cu–N2	2.205(9)	1.966(8)	Zn–N2	2.112(15)
Cu–N3	2.090(12)	2.005(7)	Zn–N3	2.196(17)
Cu–N4	1.973(11)	2.155(6)	Zn–N4	2.148(14)
Cu–N5	2.001(10)	2.108(5)	Zn–N5	2.111(13)
Bond angles (deg)				
N1–Cu–N2	79.6(4)	83.1(2)	N1–Zn–N2	79.2(6)
N1–Cu–N3	95.0(5)	162.3(3)	N1–Zn–N3	157.4(6)
N1–Cu–N4	165.8(5)	106.8(2)	N1–Zn–N4	100.7(5)
N1–Cu–N5	97.4(4)	96.98(19)	N1–Zn–N5	95.8(5)
N2–Cu–N3	85.1(5)	79.2(3)	N2–Zn–N3	79.4(6)
N2–Cu–N4	114.5(5)	129.4(4)	N2–Zn–N4	118.2(6)
N2–Cu–N5	106.8(4)	149.4(4)	N2–Zn–N5	162.8(6)
N3–Cu–N4	84.8(5)	84.7(3)	N3–Zn–N4	82.8(6)
N3–Cu–N5	164.1(5)	98.2(3)	N3–Zn–N5	106.8(6)
N4–Cu–N5	80.7(5)	80.1(2)	N4–Zn–N5	78.8(5)

**Fig. S1** The geometry configuration of complex **1–3**.

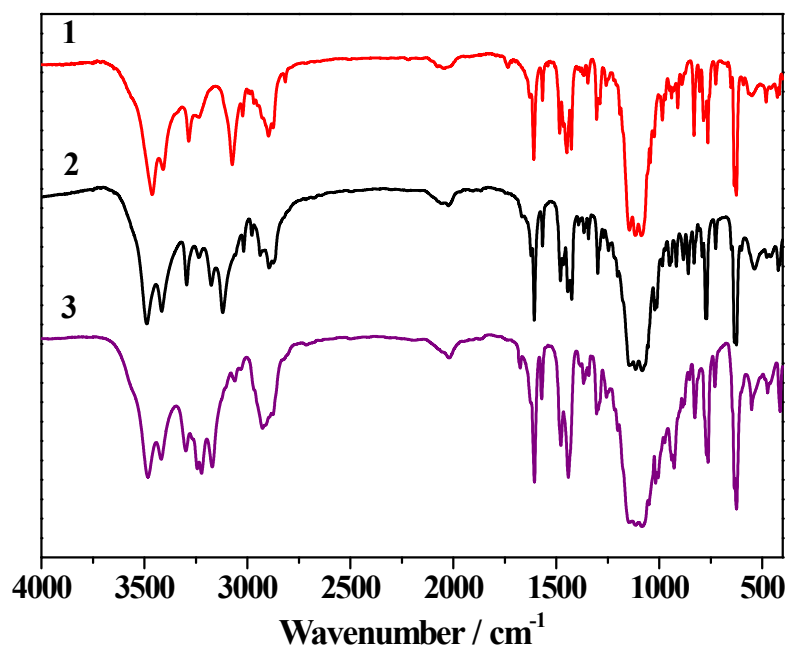


Fig. S2 The overlaid IR spectra of complex 1–3.

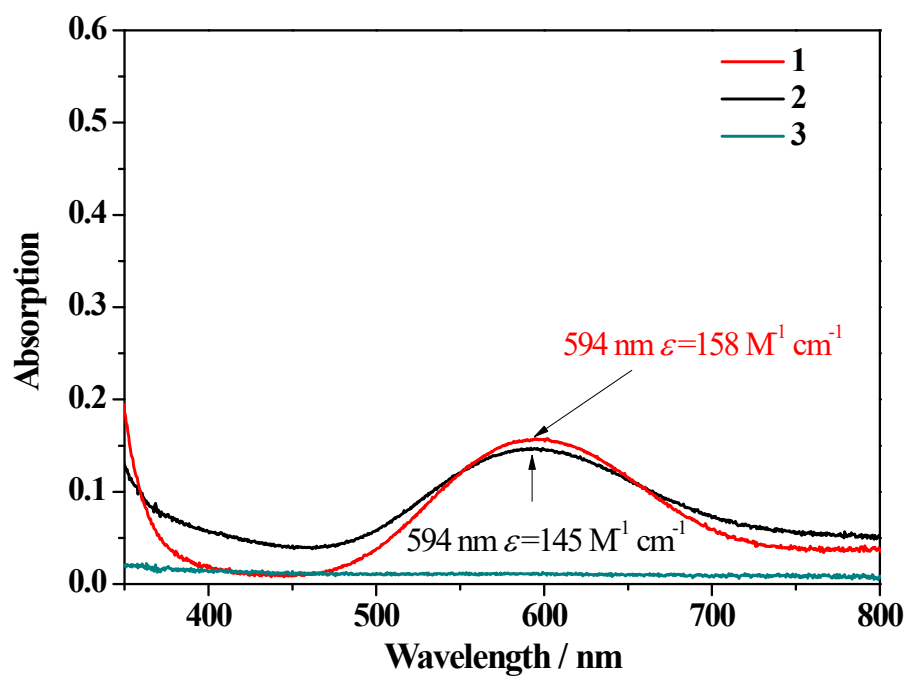


Fig. S3 UV-vis spectra of 1 mM complex 1–3 in pure water.

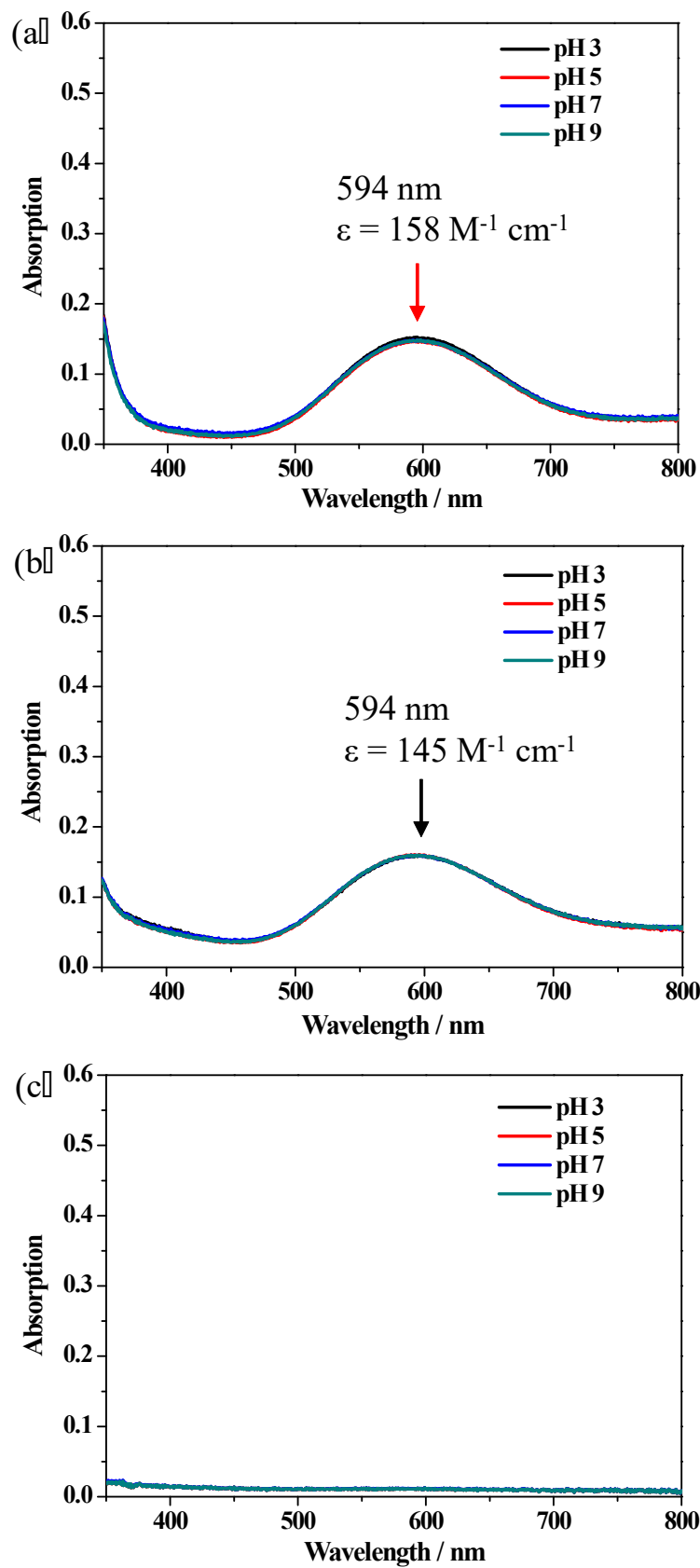


Fig. S4 UV-vis spectra of 1 mM complex 1 (a), 2 (b), 3 (c) in 0.1 M phosphate buffer solution at various pH.

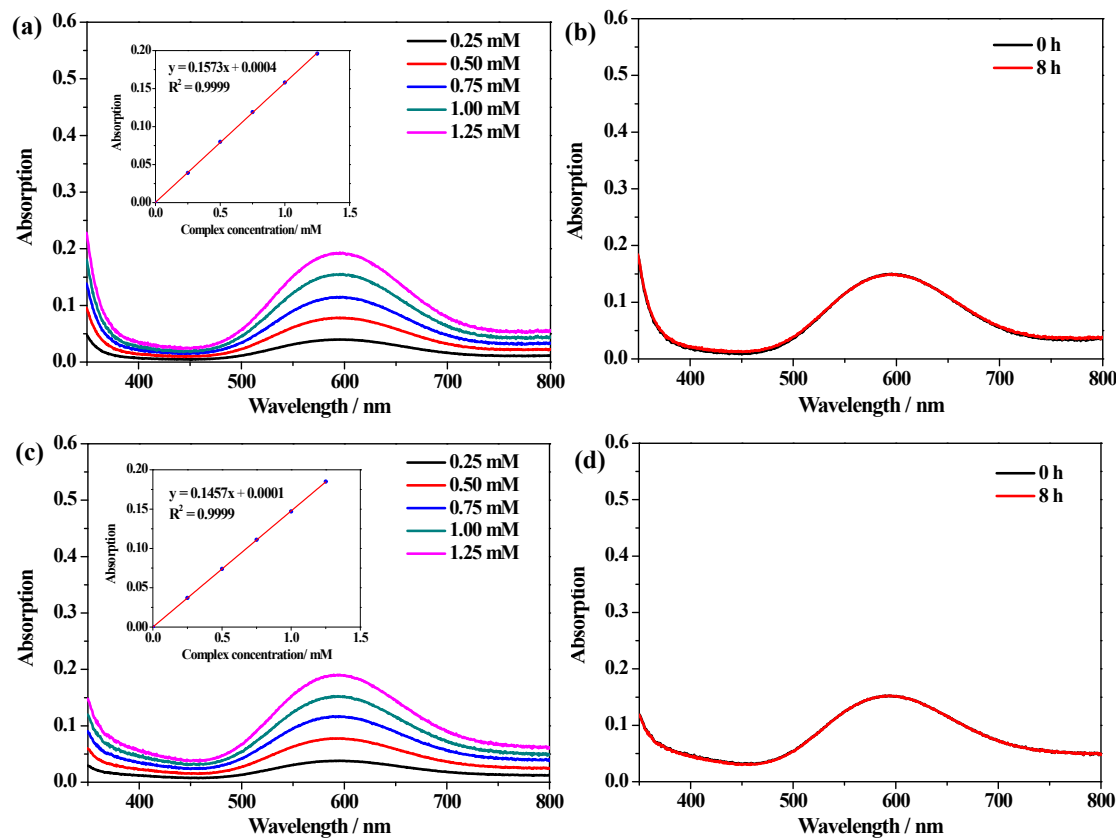


Fig. S5 Concentration-dependent UV-vis absorption spectra of complex **1** (a) and **2** (c) in 0.1 M phosphate buffer solution at pH 7.0; Time-dependent UV-vis absorption spectra of 1 mM complex **1** (b) and **2** (d) in 0.1 M phosphate buffer solution at pH 7.0.

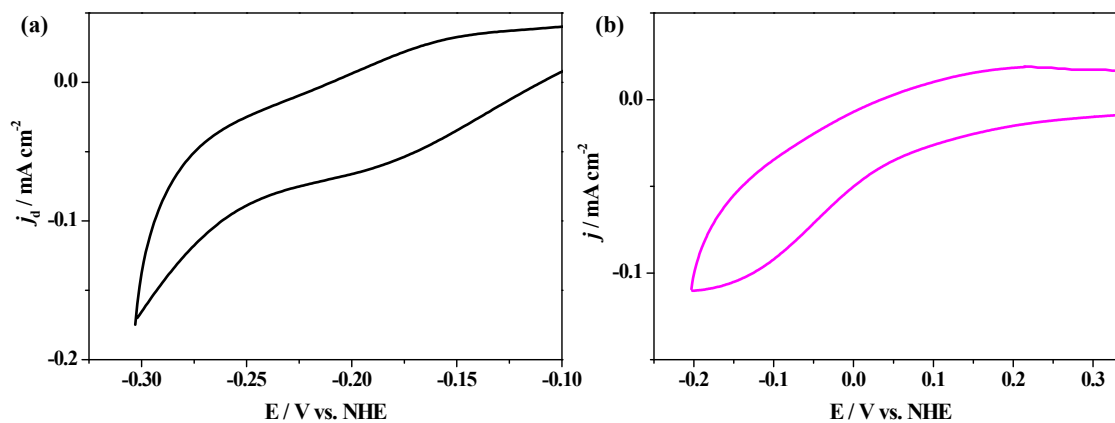


Fig. S6 The $\text{Cu}^{\text{I}}/\text{Cu}^{\text{II}}$ couple of **1** (a) and **2** (b) in 0.1 M phosphate buffer solution at pH 7.0, scan rate = 100 mV/s.

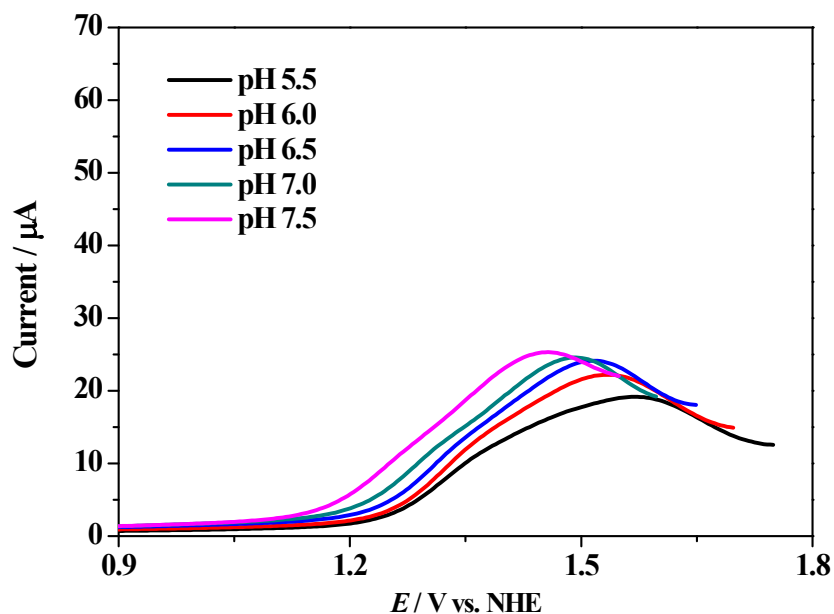


Fig. S7 DPV tests of 1.0 mM of **1** in 0.1 M phosphate buffer solution at various pH. DPVs were obtained with the following parameters: amplitude = 50 mV, step height = 4 mV, pulse width = 0.05 s, pulse period = 0.5 s and sampling width = 0.0167 s.

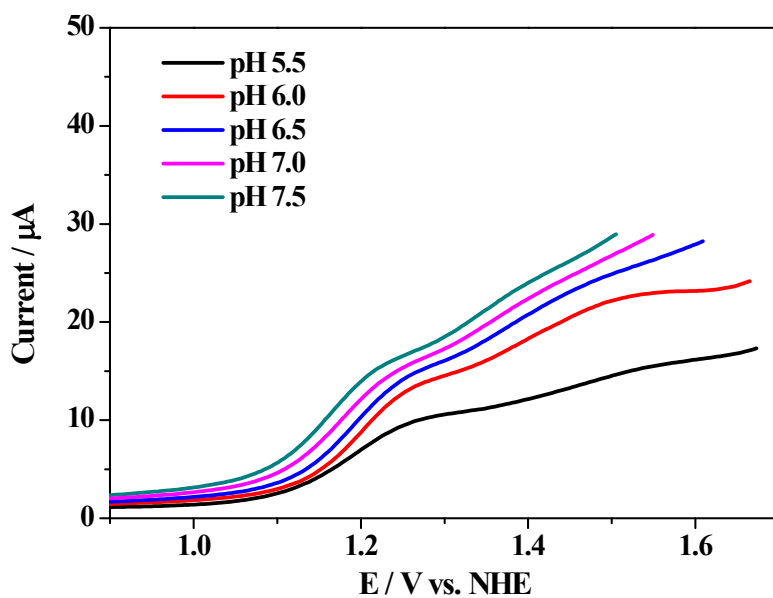


Fig. S8 DPV tests of 1.0 mM of **2** in 0.1 M phosphate buffer solution at various pH. DPVs were obtained with the following parameters: amplitude = 50 mV, step height = 4 mV, pulse width = 0.05 s, pulse period = 0.5 s and sampling width = 0.0167 s.

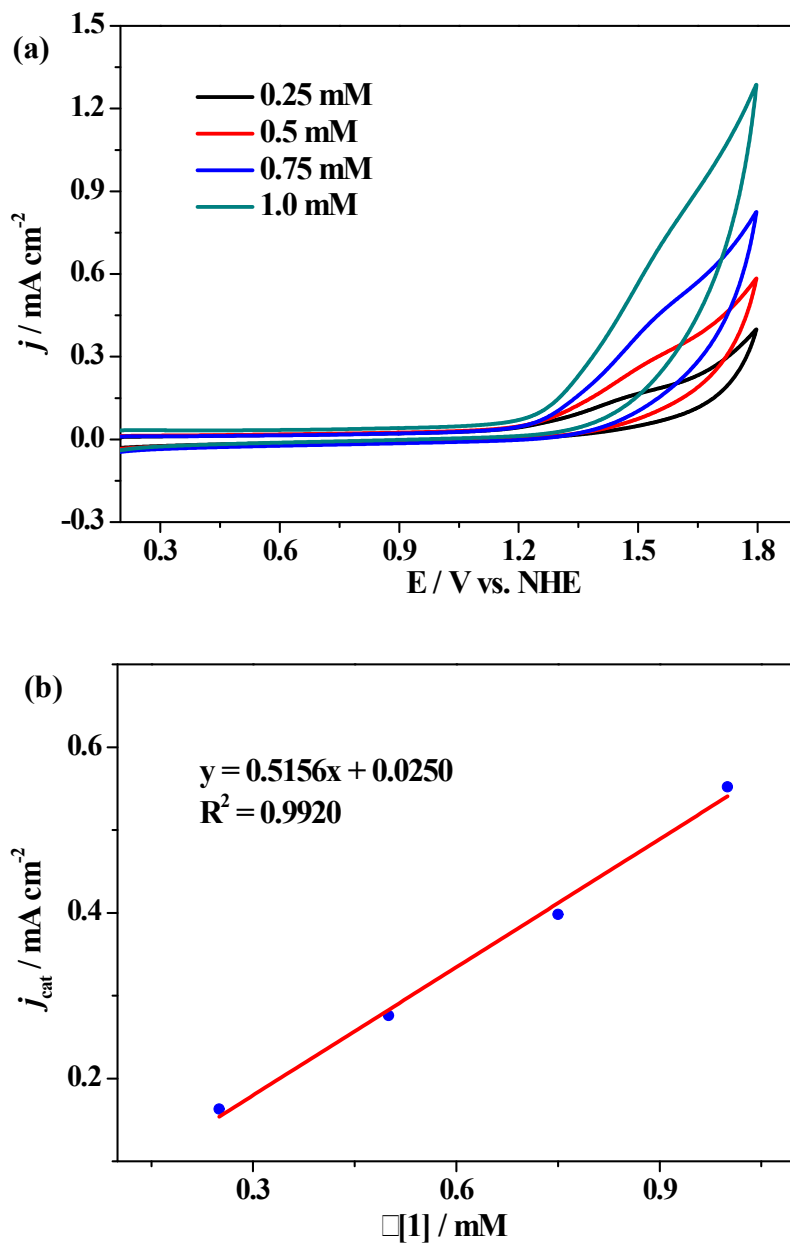


Fig. S9 Cyclic voltammograms of various concentration of **1** in 0.1 M PBSs at pH 7.0 with scan rate of 100 mV s^{-1} (a) and the dependence of j_{cat} on the concentration of **1** in 0.1 M PBSs at pH 7.0 (b).

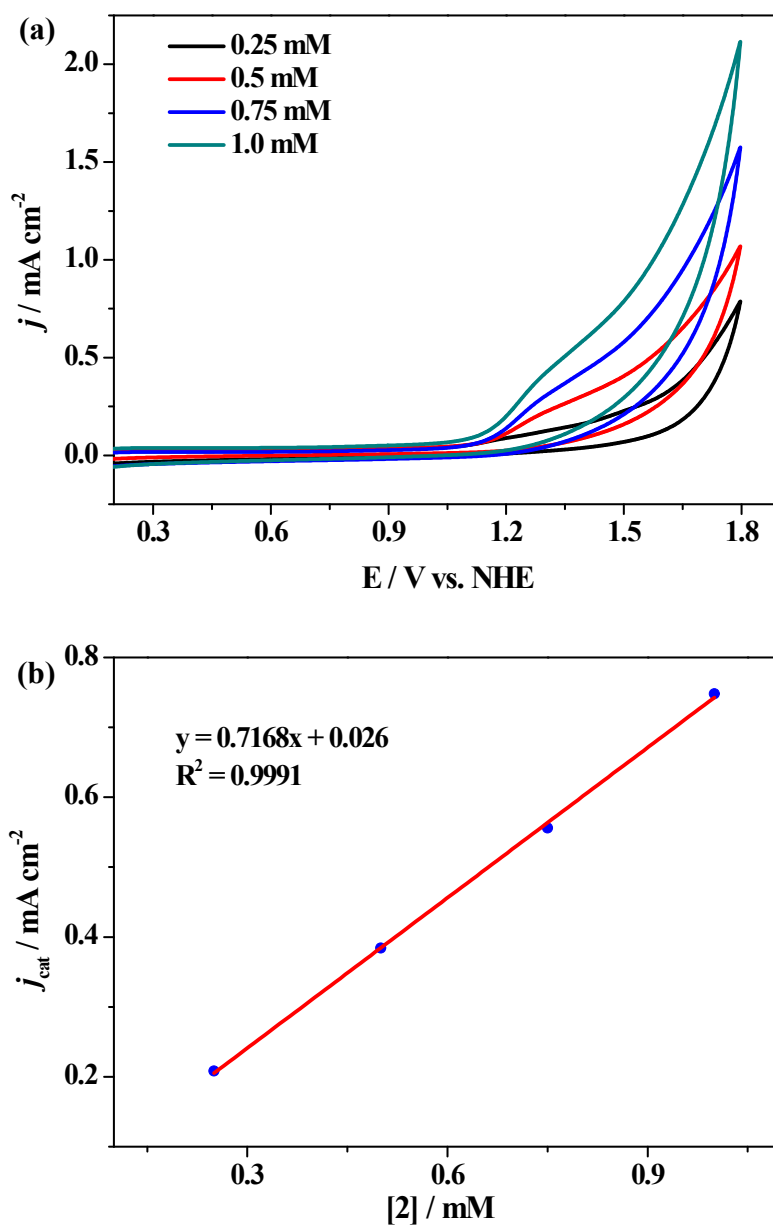


Fig. S10 Cyclic voltammograms of various concentration of **2** in 0.1 M PBSs at pH 7.0 with scan rate of 100 mV s^{-1} (a) and the dependence of j_{cat} on the concentration of **2** in 0.1 M PBSs at pH 7.0 (b).

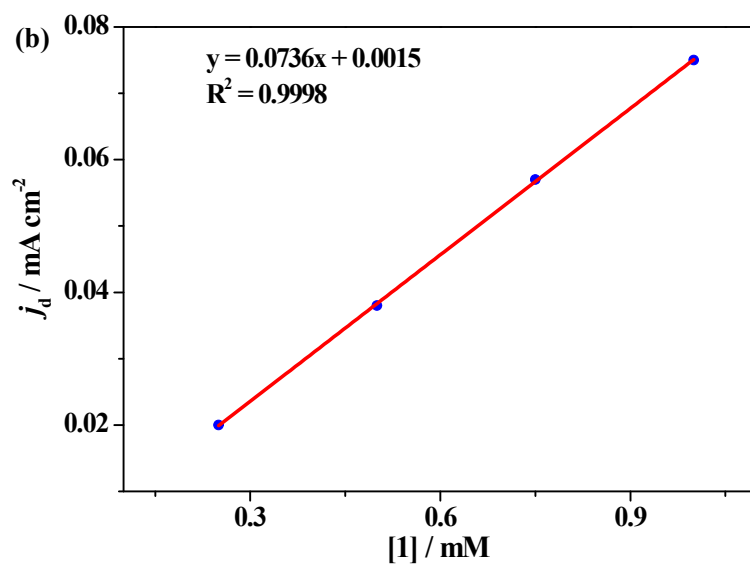
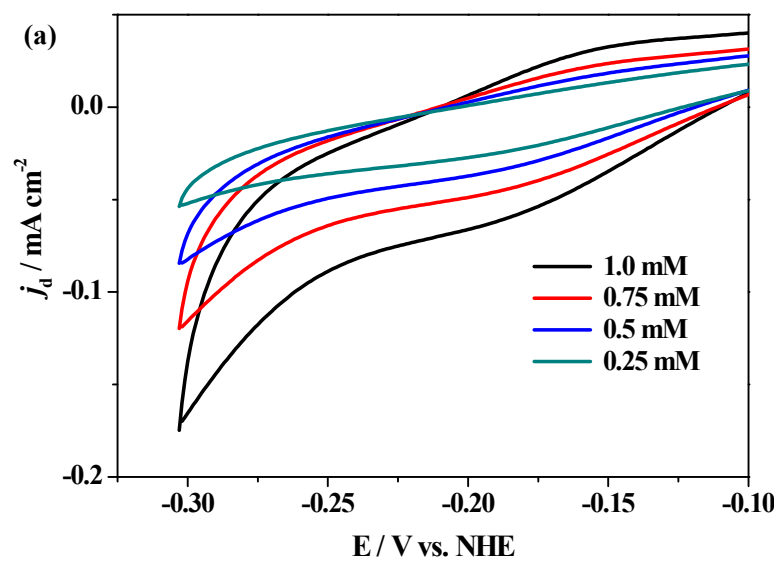


Fig. S11 Cyclic voltammograms of 1.0 mM of **1** with various concentration (a) and dependence of reduction wave current density of the $\text{Cu}^{\text{I}}/\text{Cu}^{\text{II}}$ couple of **1** on its concentration (b).

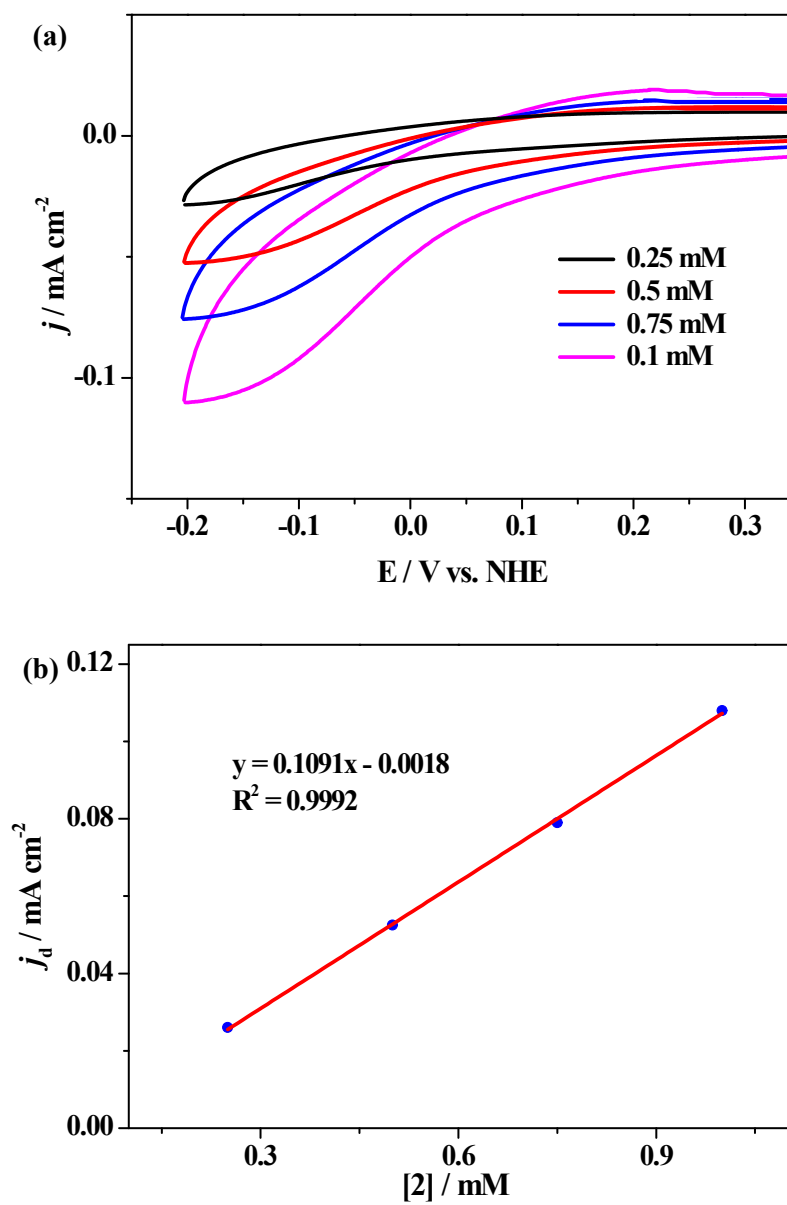


Fig. S12 Cyclic voltammograms of 1.0 mM of **2** with various concentration (a) and dependence of reduction wave current density of the Cu^I/Cu^{II} couple of **2** on its concentration (b).

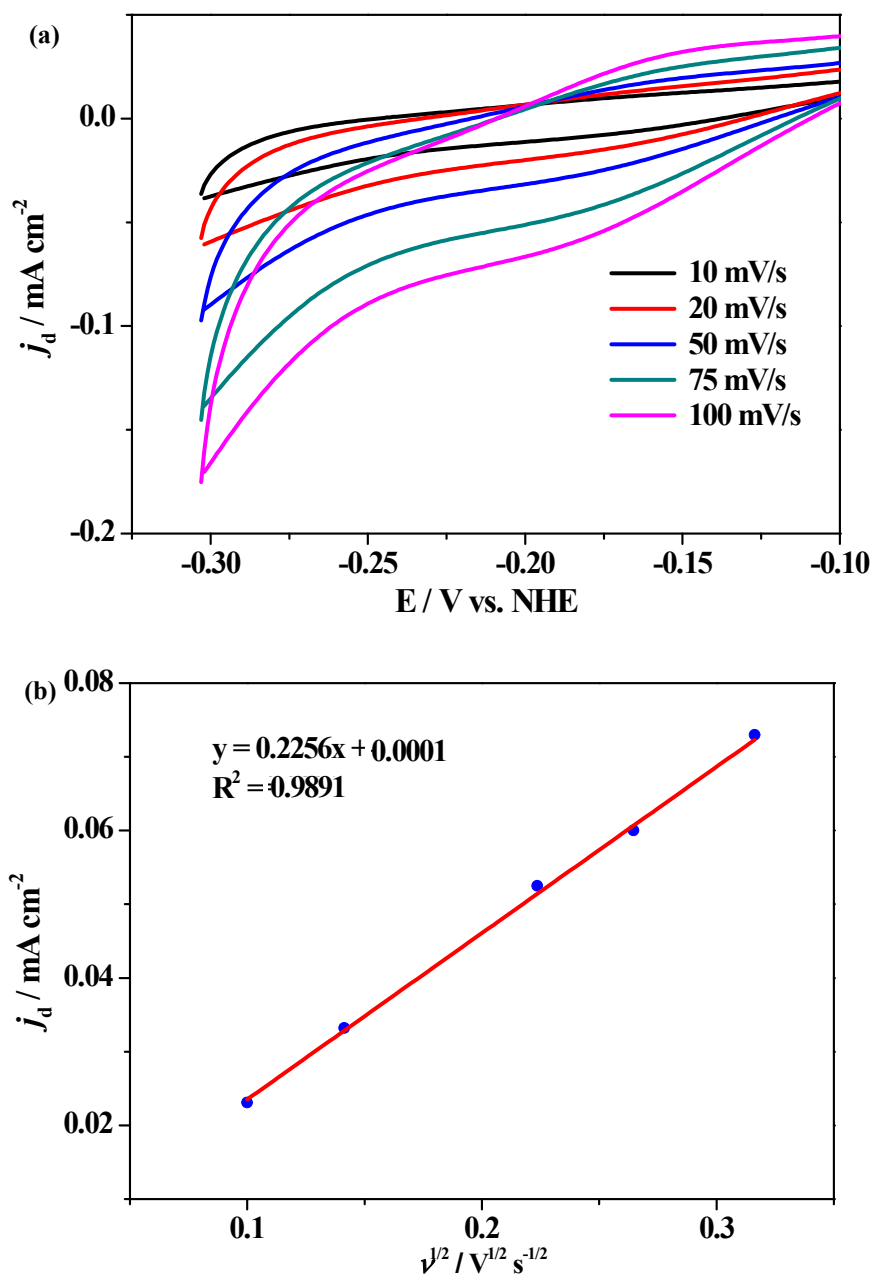


Fig. S13 CV of 1.0 mM of **1** with various scan rate (a) and dependence of reduction wave current density of the $\text{Cu}^{\text{I}}/\text{Cu}^{\text{II}}$ couple of **1** on the square root of scan rates (b).

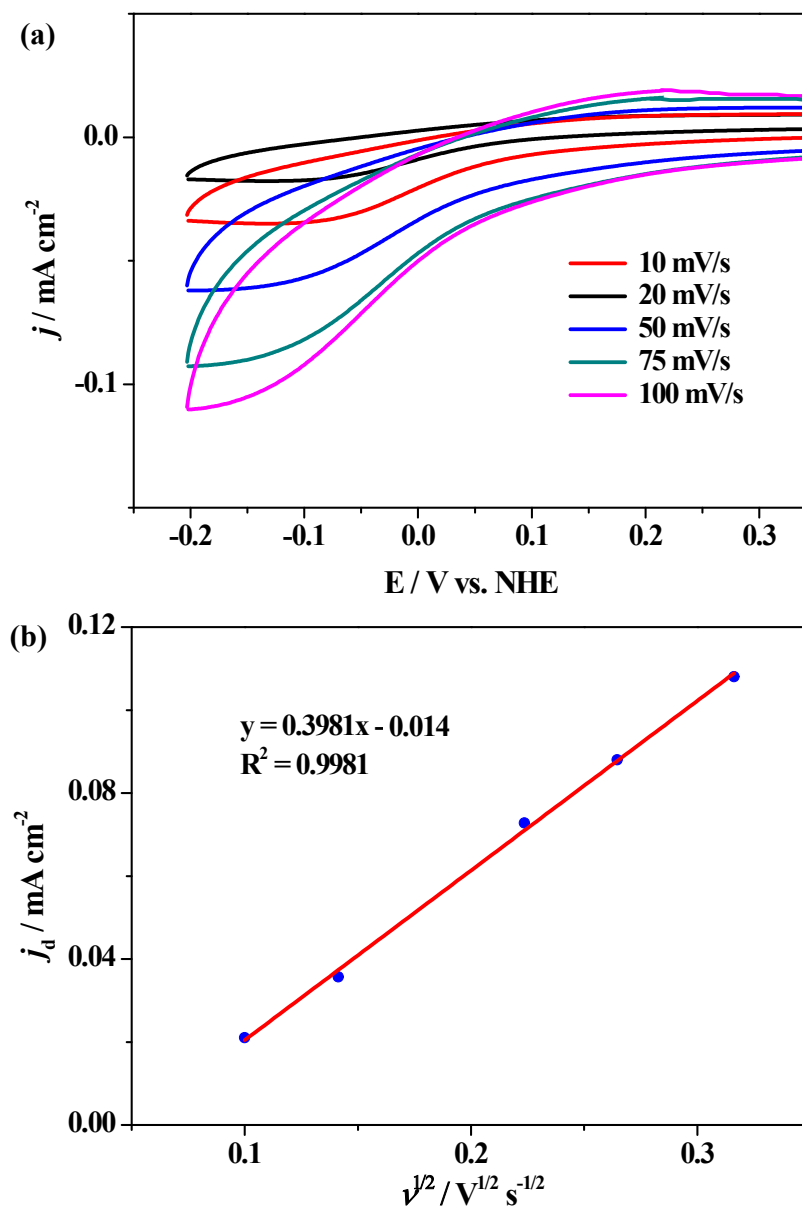


Fig. S14 CV of 1.0 mM of **2** with various scan rate (a) and dependence of reduction wave current density of the $\text{Cu}^{\text{I}}/\text{Cu}^{\text{II}}$ couple of **2** on the square root of scan rates (b).

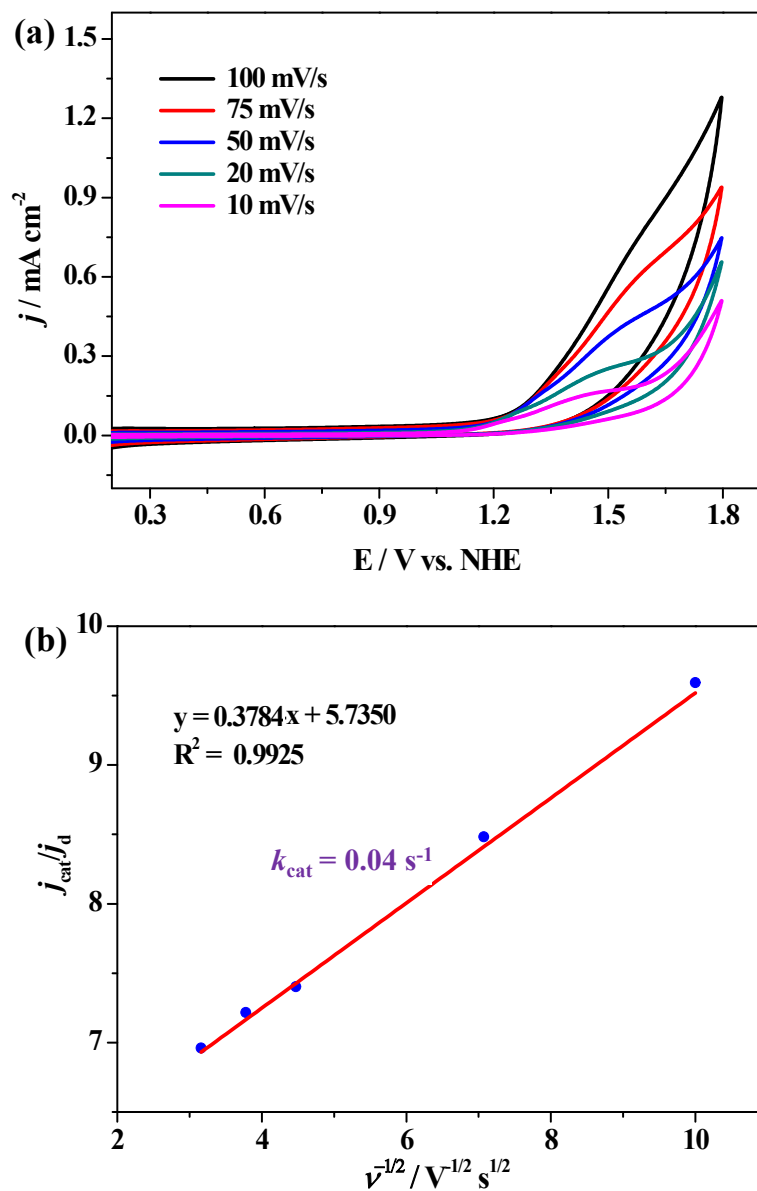


Fig. S15 CV of 1.0 mM of **1** in 0.1 M PBSs with scan rate varying from 10 to 100 mV s⁻¹ (a) and plots of the ratio of j_{cat} to j_d of **1** versus the reciprocal of the square root of the scan rate (b).

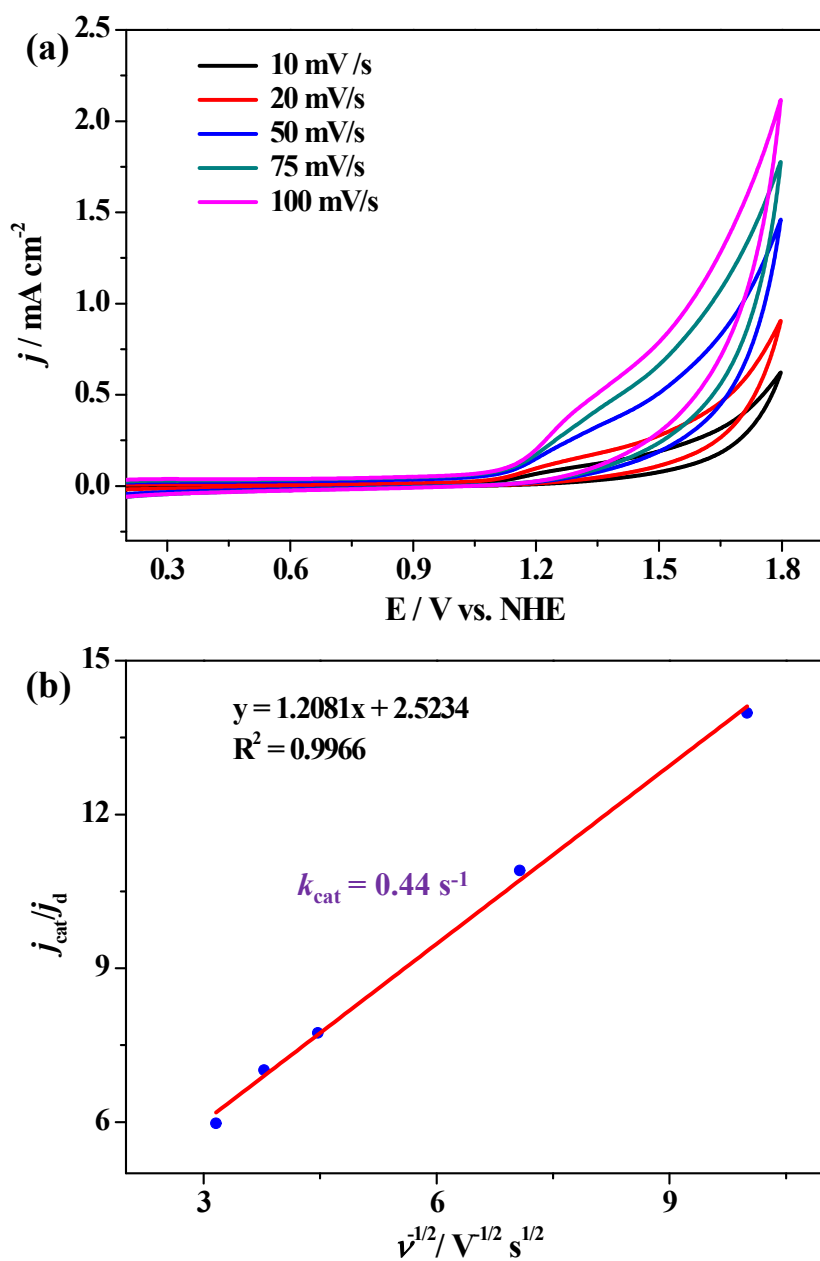


Fig. S16 CV of 1.0 mM of **2** in 0.1 M PBSs with scan rate varying from 10 to 100 mV s⁻¹ (a) and plots of the ratio of j_{cat} to j_{d} of **2** versus the reciprocal of the square root of the scan rate (b).

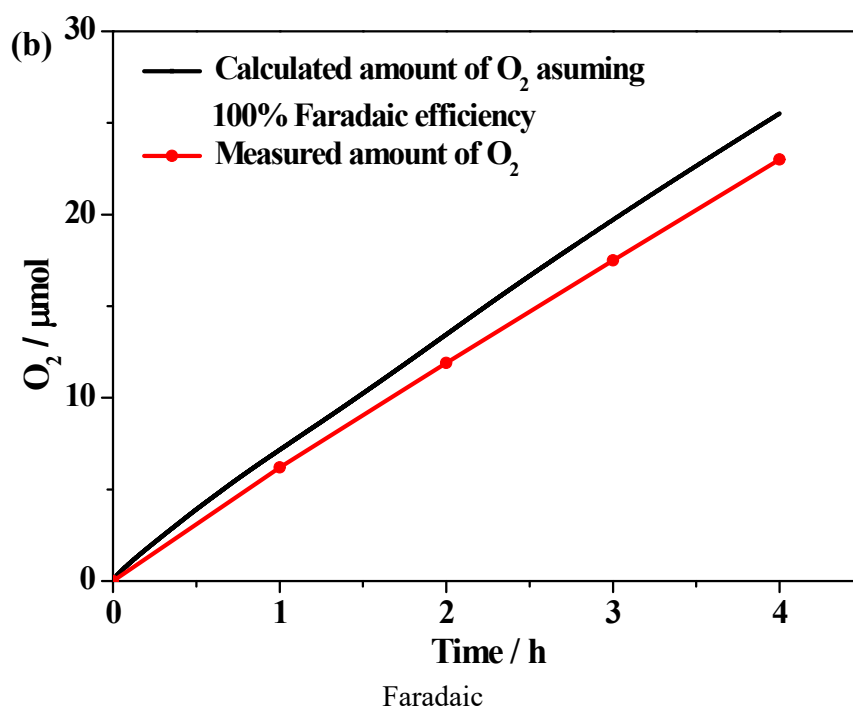
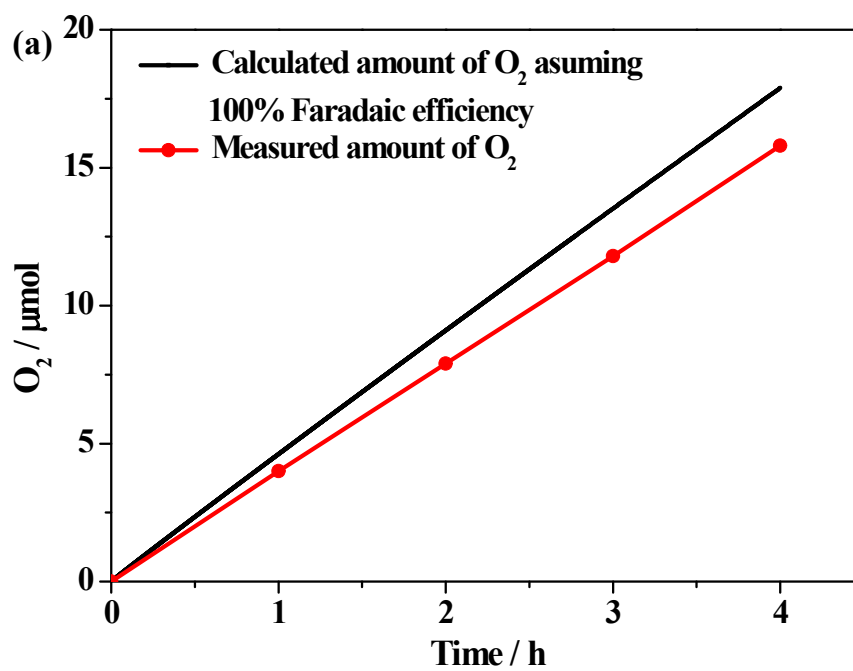


Fig. S17 Faradaic efficiency of O₂ evolution for **1** (a) and **2** (b) under 4 h of electrolysis at 1.70 V vs. NHE in 0.1 M PBS at pH 7.0.

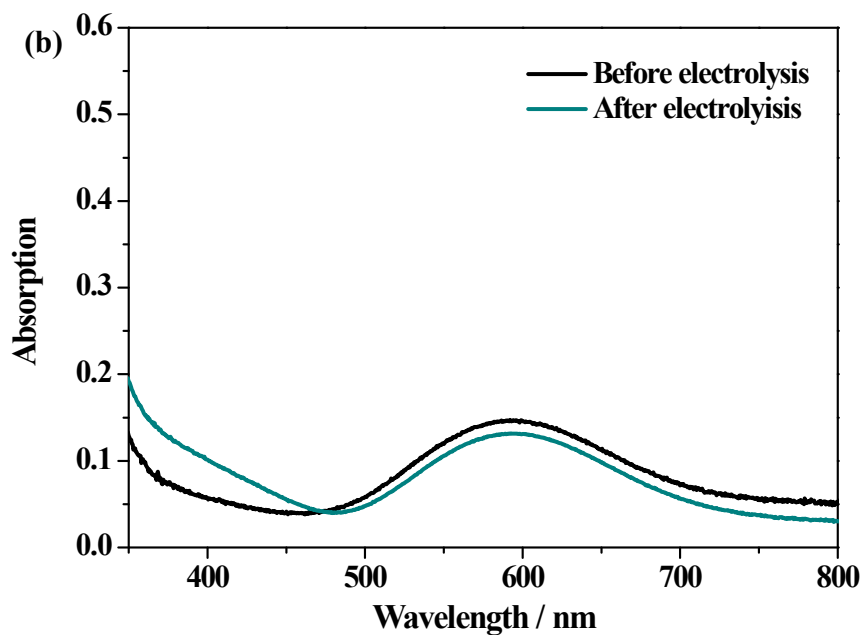
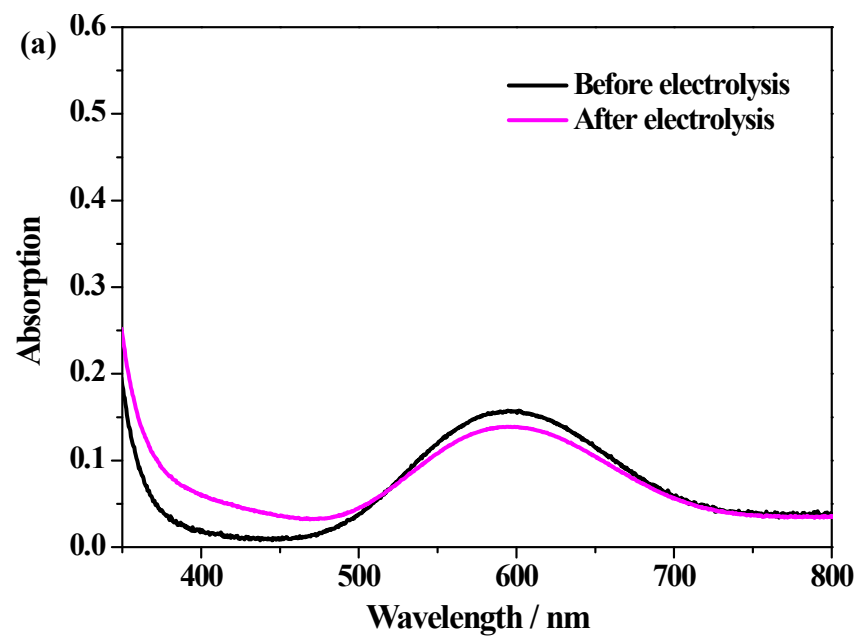


Fig. S18 UV-visible measurements of **1** (a) and **2** (b) in 0.1 M PBS at pH 7.0 before and after 4 h controlled potential electrolysis at 1.70 V vs. NHE. Initial concentration of **1** and **2** was 1 mM.

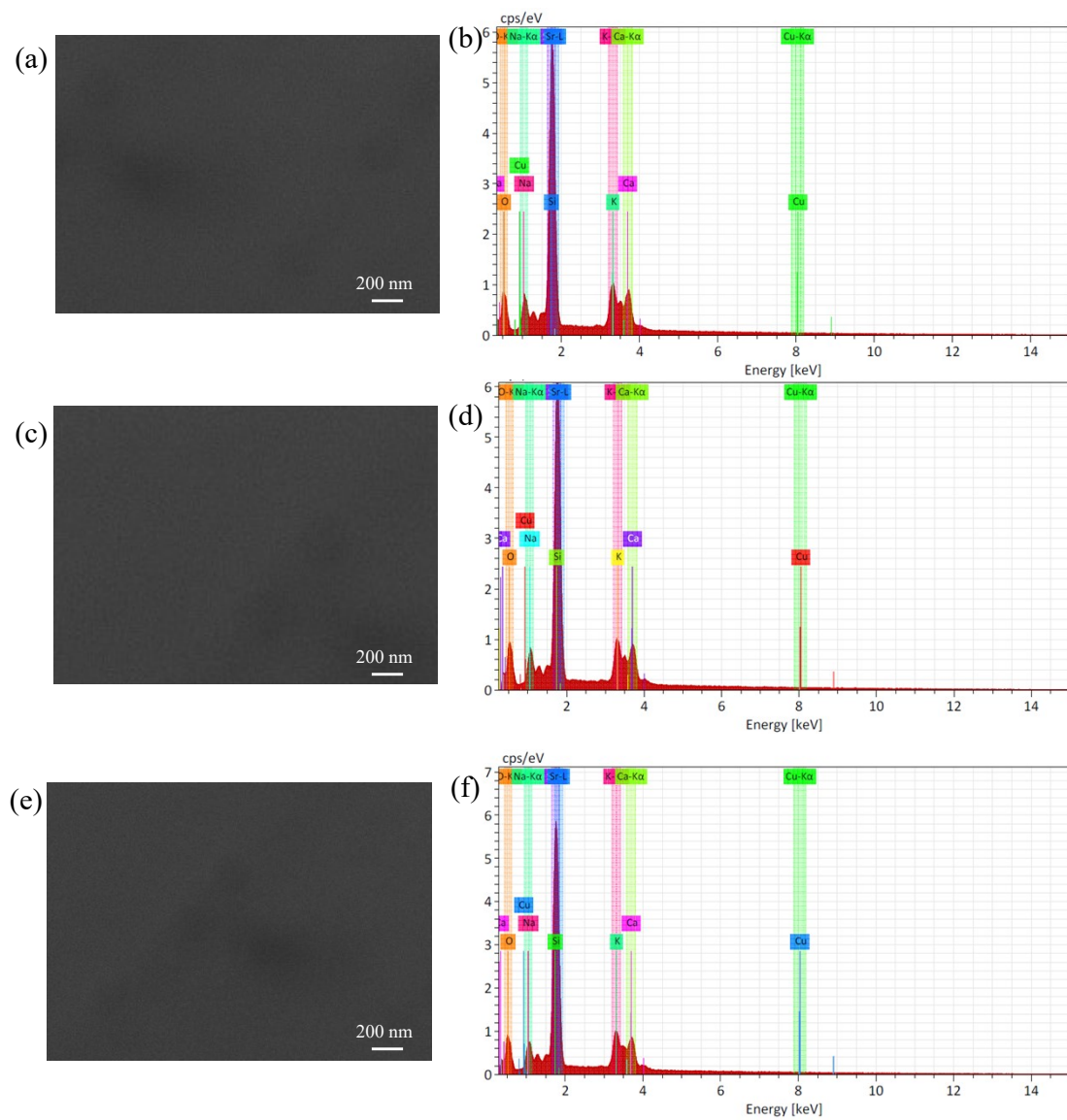


Fig. S19 SEM images and EDX analysis result of the surface of ITO electrode before (a and b) and after 4 h CPE experiments of **1** (c and d) and **2** (e and f) in 0.1 M phosphate buffer solution at neutral pH.